Electronic supplementary information

Ice-templated Assembly Strategy to Construct Graphene Oxide/Boron Nitride Hybrid Porous Scaffolds in Phase Change Materials with Enhanced Thermal Conductivity and Shape Stability for Light-thermal-electric Energy Conversion

Jie Yang, Li-Sheng Tang, Rui-Ying Bao, Lu Bai, Zheng-Ying Liu, Wei Yang*, Bang-Hu Xie, Ming-Bo Yang

College of Polymer Science and Engineering, Sichuan University, State Key Laboratory of Polymer Materials Engineering, Chengdu 610065, Sichuan, China.

*Correspondence - weiyang@scu.edu.cn

Synthesis of Graphite oxide

Graphite oxide was synthesized from natural graphite flakes with an average particle size of 200 meshes and a purity of over 99.9% by a modified Hummers method. Concentrated H_2SO_4 (150 ml) was heated to 90 °C in a 500 ml three-necked, round-bottomed flask. $K_2S_2O_8$ (20 g) and P_2O_5 (20 g) were added into the solution in sequence under continuous stirring until the reactants are completely dissolved. The mixture was then cooled down to 80 °C. Graphite powder (24 g) was added to above mixture, and the resulting mixture was kept at 80 °C for 4.5 h. After that the mixture was diluted with 1 L distilled water and left overnight. The mixture was then filtered and washed to remove all traces of acid, and the obtained pretreated graphite was transferred to a drying dish and left overnight under ambient conditions. Next, the pretreated graphite (6 g) was added to a 1 L flask with concentrated H_2SO_4 (230 ml) in an ice bath, and $KMnO_4$ (30 g) was added slowly under continuous stirring. This mixture was then allowed to react at 35 °C for 2 h, after which distilled water (460 ml) was slowly added. Note that an ice bath must be used in this phase to maintain the temperature to be below 50 °C because the addition of water caused the temperature of the mixture to rise rapidly. When the temperature of the mixture kept constant, the mixture was transferred to a beaker with 1.4 L distilled water and stirred for another 2 h, and then 25 mL of 30% H_2O_2 was added to the mixture, resulting in a brilliant yellow color. After the mixture was left overnight, the supernatant was filtered. The remaining precipitate was washed

with 5% HCl aqueous solution to remove the metal ions followed by continually washing with deionized water to remove the acid until the pH is neutral.

Preparation of PEG/BN composite PCMs

For comparison, PEG/BN samples were prepared by a solution blending method. Firstly, a certain amount of BN powder was dispersed in absolute ethanol with the aid of ultrasonic bath treatment for 30 min. PEG was then added, and the mixture was vigorously stirred at 90 °C for 3 h to evaporate the solvent. Finally, the products were dried in a vacuum oven to a constant weight at 50 °C. The obtained PEG based composite PCMs containing different contents of BN were labled as SB10, SB15 and SB20, respectively.

Characterizations

The Raman spectra (Fig. S1a) and XRD pattern (Fig. S1b) of both pristine graphite and GO show significant differences. Pristine graphite displays two sharp characteristic peaks at ~ 1,579 cm^{-1} (G peak) and ~ 2,721 cm^{-1} (2D peak), while the 2D peak of GO disappears, and a new peak emerges at ~ 1,348 cm^{-1} (D peak), confirming lattice distortions induced by oxidation. The XRD pattern (Fig. S1b) of GO indicates that the interlayer spacing GO increases dramatically due to the attachment of various oxygen-containing functional groups on the C–C basal planes. The UV-vis spectra of GO presents a strong absorption peak at ~ 232 nm (π- π* transitions of the conjugation domains) and a weak shoulder peak at ~ 300 nm (n-π* transitions of the carbonyl groups), as shown in Fig. S1c.[1-3]

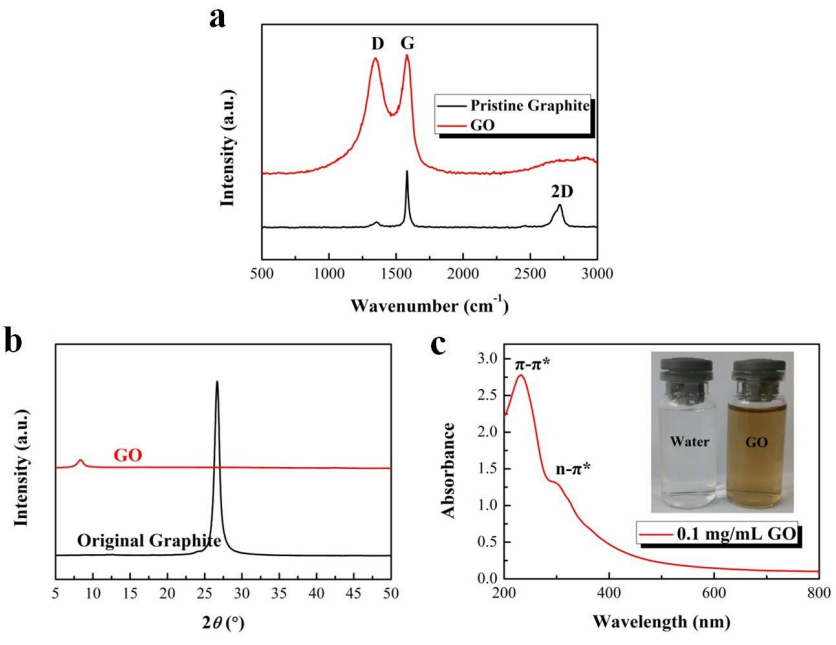

Fig. S1 (a) Raman spectra, (b) XRD pattern and (c) UV-vis absorption spectrum of GO.

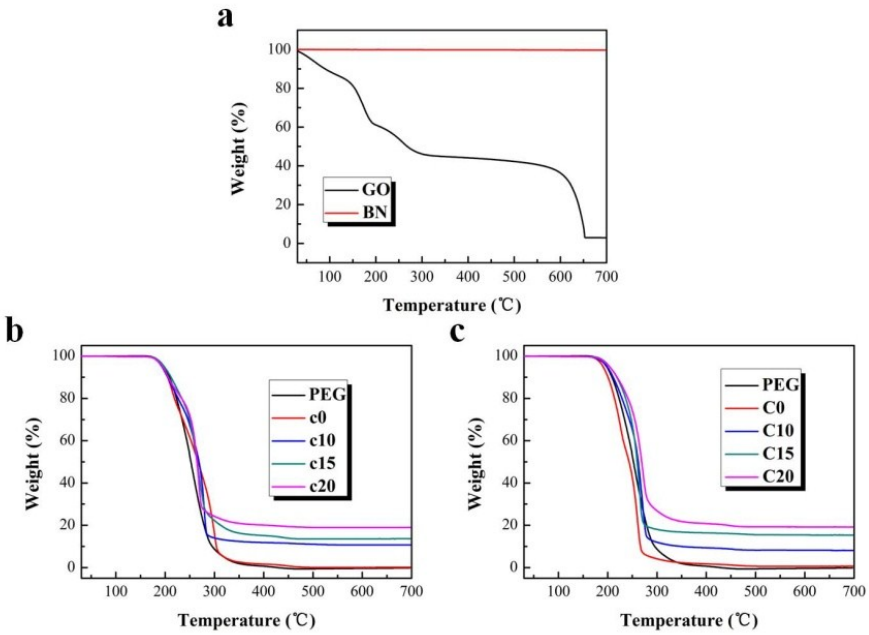

Fig. S2 TGA curves of (a) GO and BN, (b) the composite PCMs with HPSs obtained from low freezing temperature (~ -170 °C) and (c) the composite PCMs with HPSs obtained from high freezing temperature (~ -10 °C).

The BN loading in the composite PCMs is determined by TGA under air atmosphere. Fig. S2 shows GO, PEG, c0 and C0 almost completely decompose during the measurement, while pristine BN exhibits high thermal stability up to 700 °C without any decomposition. Therefore, the weight of residue after burning could be regarded as the BN loading in the composite PCMs, as listed in Table S1.

Table S1 The content of BN in the composite PCMs.

Samples	c10	c15	c20	C10	C15	C20
BN (wt%)	10.8	13.7	19.0	8.1	15.4	19.2

The HPSs obtained from lower freezing temperature exhibit lightweight and desired shapes, and sample s20 with dimensions of 35 mm in diameter and ~5 mm in thickness can bear the compression generated by 500 grams force, as shown Fig. S3.

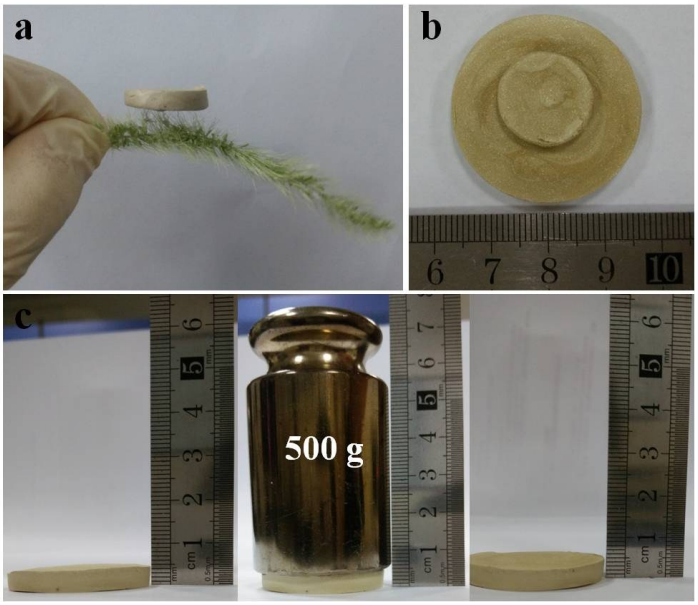

Fig. S3 Digital photograph of (a) s20 standing on a flower like dog's tail and (b) s20 with diverse shapes. (c) Strong s20 sample (35 mm in diameter and ~5 mm in thickness) bearing the compression generated by 500 grams force.

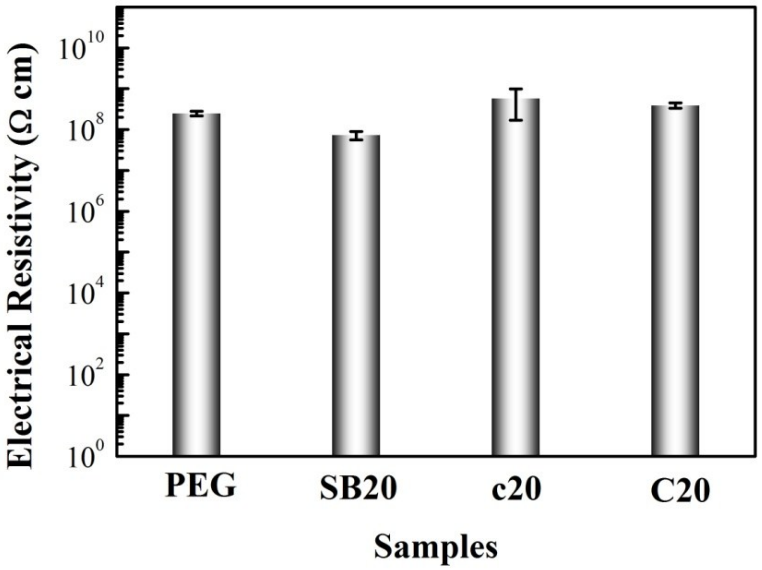

Fig. S4 Volumetric electrical resistivity of PEG, SB20, c20 and C20.

Owing to the superior electrical insulation of boron nitride (BN) and (GO), the volumetric electrical resistivity of composite PCMs is maintained at the same level as that of pure PEG, as shown in Fig. S4.

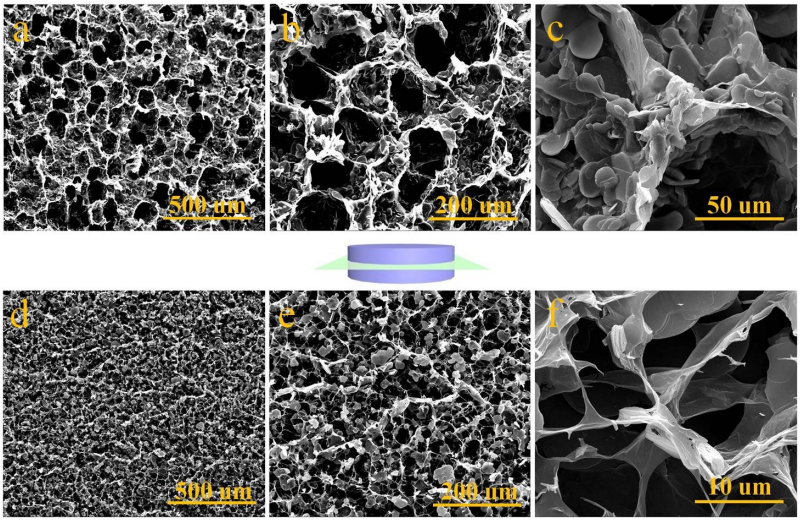

Fig. S5 The horizontally cross-sectional SEM images of (a)-(c) C10 and (d)-(f) c10.

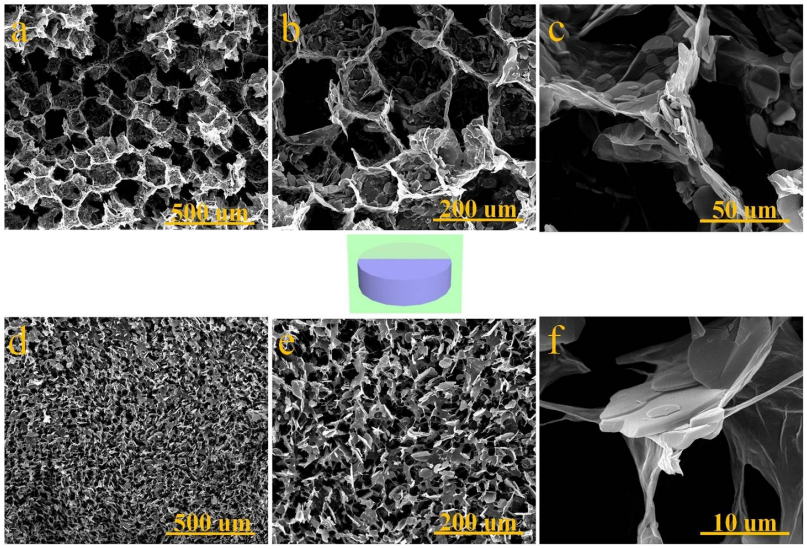

Fig. S6 The perpendicularly cross-sectional SEM images of (a)-(c) C10 and (d)-(f) c10.

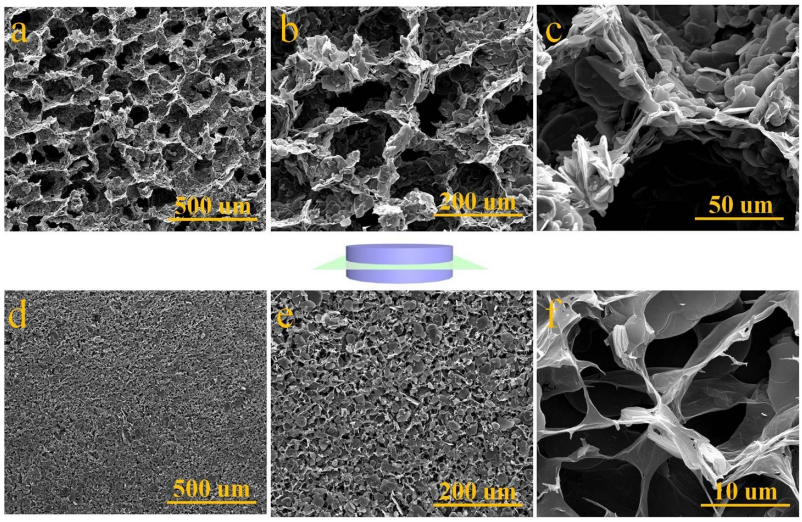

Fig. S7 The horizontally cross-sectional SEM images of (a)-(c) C15 and (d)-(f) c15.

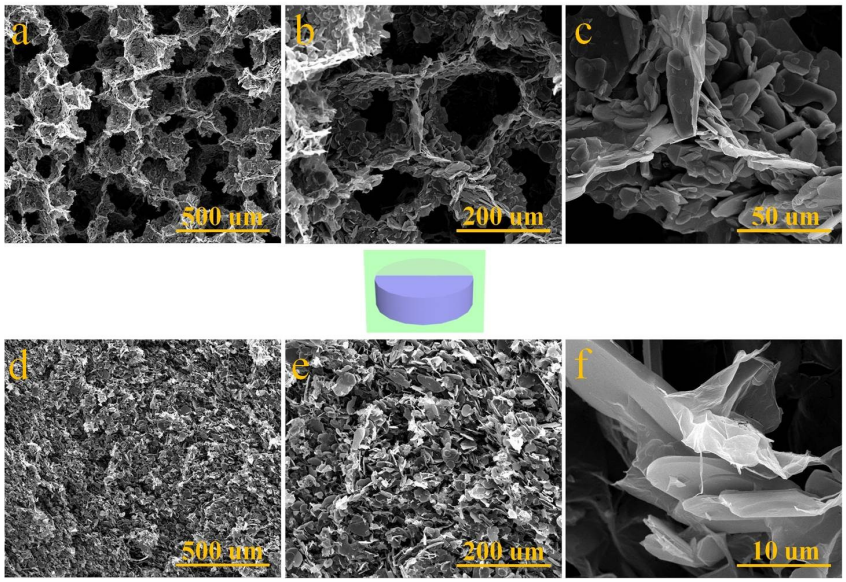

Fig. S8 The perpendicularly cross-sectional SEM images of (a)-(c) C10 and (d)-(f) c10.

Fig. S5-S8 describe the horizontally and perpendicularly cross-sectional morphologies of s10, s15, S10 and S15 subjected to different freezing temperatures. It can be clearly seen that the micropores become sparser and the pore size decreases with the decrease of freezing temperature in both horizontal and pendicular derections. On the basis of the SEM images, BN agglomerates linked by GO form an ordered thermally conductive network (like cellular), leading to largely enhancing thermal conductivity for both HPSs and corresponding composite PCMs.

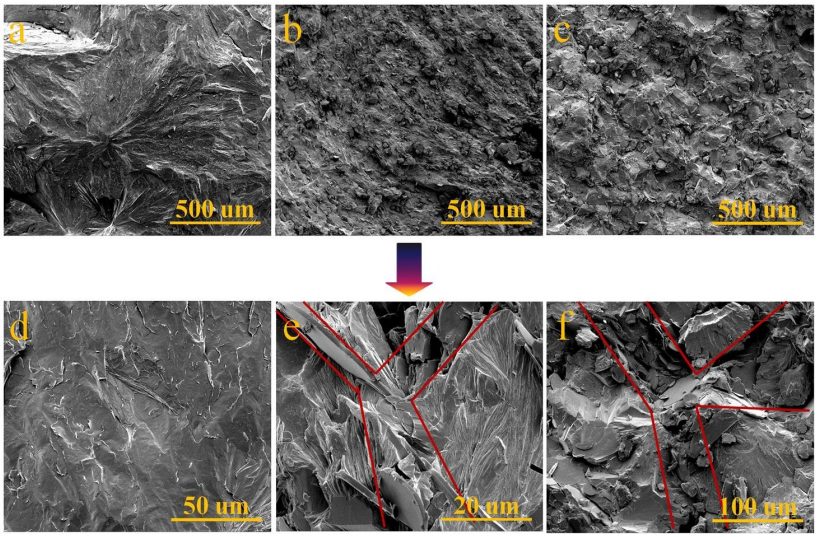

Fig. S9 The perpendicularly cross-sectional SEM images of (a), (d) PEG, (b), (e) c20 and (c), (f) C20 (The red part represents the thermally conductive pathway formed by BN in the composite PCMS).

The perpendicularly cross-sectional SEM images of PEG c20 and C20 are shown in Fig. S9, showing the ordered 3D networks are maintained well after the infiltration of PEG. In sharp constrast, compared with pure PEG (in Fig. S9a and d), c20 (in Fig. S9b and e) and C20 (in Fig. S9c and f) exhibit rougher fracture surface due to the introduction of a large amount of BN. Note that the thermally conductive pathway in C20 is more unobstructed and perfect than that in c20 at the similar content of BN, which is in accordance with the results of SEM images shown in Fig. 5, 6 and 12c.

Fig. S10 shows that the introduction of ultra-low content of GO in the PEG based PCMs has no obvious influence on the thermal conductivity of the composite PCM, which can be explained by the fact that the thermal conductivity of GO is significantly reduced with the oxygen coverage increasing.[4]

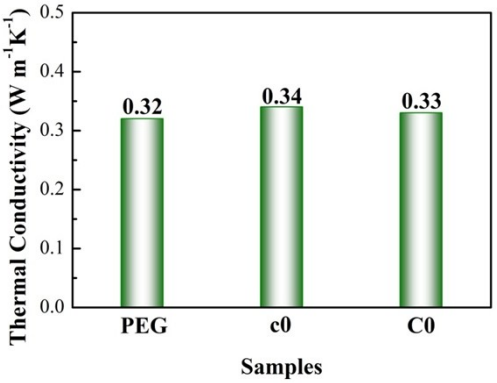

Fig. S10 Thermal conductivity of PEG, c0 and C0.

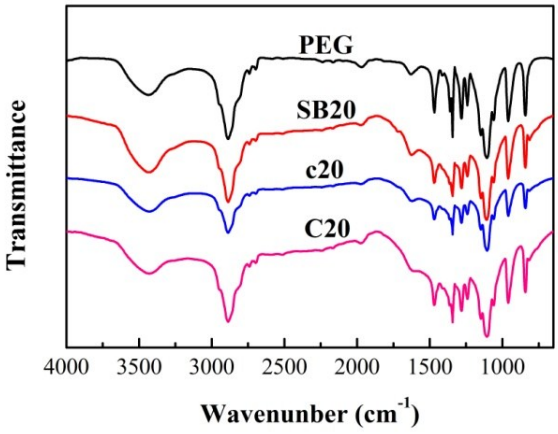

Fig. S11 FTIR spectrum of PEG, SB20, c20 and C20.

Owing to the intermolecular hydrogen bonding interaction between PEG and GO,[5] the most absorption peaks of the functional groups of PEG appeared with only a slight shift of peak positions in c20 and C20, as shown in Fig. S11.

To ensure reproducibility of DSC results, each group of samples has been tested repeatly, and the mean value and standard deviation are obtained, as shown in Fig. S12.

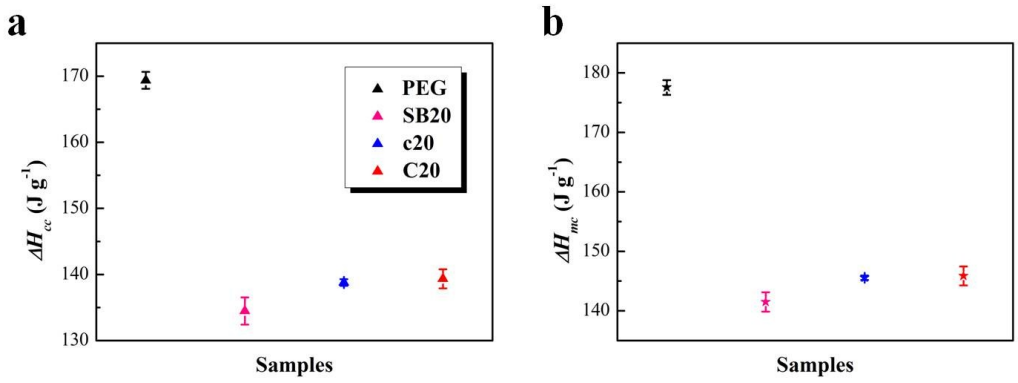

Fig. S12 (a) crystallization (ΔH_{mc}) and (b) melting (ΔH_{cc}) enthalpy of PEG, SB20, c20 and C20

References

1 S. Stankovich, D. A. Dikin, R. D. Piner, K. A. Kohlhaas, A. Kleinhammes, Y. Jia, Y. Wu, S. T. Nguyen and R. S. Ruoff, *Carbon*, 2007, **45**, 1558-1565.

2 J. Cao, G. Q. Qi, K. Ke, Y. Luo, W. Yang, B. H. Xie and M. B. Yang, *J. Mater. Sci.*, 2012, **47**, 5097-5105.

3 L. Peng, Z. Xu, Z. Liu, Y. Wei, H. Sun, Z. Li, X. Zhao and C. Gao, *Nat. commun.*, 2015, **6**, 5716.

4 X. Mu, X. Wu, T. Zhang, D. B. Go and T. Luo, *Sci. rep.*, 2014, **4**, 3909.

5 C. Wang, L. Feng, H. Yang, G. Xin, W. Li, J. Zheng, W. Tian and X. Li, *Phys. chem. chem. phys.*, 2012, **14**, 13233-13238.